

# UC San Diego

## UC San Diego Previously Published Works

### Title

Comparing solar inverter design rules to subhourly solar resource simulations

### Permalink

<https://escholarship.org/uc/item/9s70h75z>

### Journal

Journal of Renewable and Sustainable Energy, 15(5)

### ISSN

1941-7012

### Authors

Zapata, Mónica Zamora

Lappalainen, Kari

Kankiewicz, Adam

et al.

### Publication Date

2023-09-01

### DOI

10.1063/5.0151042

### Copyright Information

This work is made available under the terms of a Creative Commons Attribution License, available at <https://creativecommons.org/licenses/by/4.0/>

Peer reviewed

**1 Comparing solar inverter design rules to subhourly solar resource simulations**

2 Mónica Zamora Zapata,<sup>1</sup> Kari Lappalainen,<sup>2</sup> Adam Kankiewicz,<sup>3</sup> and Jan Kleissl<sup>4</sup>

3 <sup>1</sup>*Departamento de Ingeniería Mecánica, Universidad de Chile,*

4 *Chile*

5 <sup>2</sup>*Unit of Electrical Engineering, Tampere University, Finland*

6 <sup>3</sup>*Black & Veatch, USA*

7 <sup>4</sup>*Department of Mechanical and Aerospace Engineering, University of California San*  
8 *Diego, USA*

9 (\*mzamora@uchile.cl)

10 (Dated: 17 August 2023)

11 The input of a solar inverter depends on multiple factors: the solar resource, weather condi-  
12 tions, and control strategies. Traditional design calculations specify the maximum current  
13 either as 125% of the rated module current or as the maximum 3 hour average current from  
14 hourly simulations over a typical year, neglecting extreme irradiance conditions: cloud en-  
15 hancement events that usually last minutes. Inverter power-limiting control strategies usu-  
16 ally prevent extreme events to cause strong currents at the inverter but in some cases, they  
17 can fail, leading to high currents. In this study, we aim to report how frequent and strong  
18 these high currents could be. We use 10 years of 1 minute data from 7 stations across the  
19 United States to estimate the PV string output through modeling the short-circuit current  
20  $I_{sc}$ , and the maximum-power point current  $I_{mp}$ , and compare them to traditional inverter  
21 design values. We consider different configurations: minutely to hourly resolution; 5 min  
22 to 3 h averaging time intervals; monofacial and bifacial modules (with a case of enhanced  
23 albedo); and 3 fixed-tilt angles and horizontal single-axis tracking. The bifacial modules  
24 with enhanced albedo lead to the highest currents for 1 min data, exceeding 3 hour aver-  
25 ages by 53% for  $I_{sc}$  and 38% for  $I_{mp}$ . The 3 hour average maxima surpass the conservative  
26 125% design rule for bifacial modules. Inverter ratings at either a 200% of the rated cur-  
27 rent or 1.55 times the 3 hour maximum could withstand all 1 events regardless of control  
28 strategies.

29 **I. INTRODUCTION**

30 Solar photovoltaic (PV) plants have grown strongly in the past decade, reaching 738 GW of  
31 installed capacity worldwide in 2021, and capacity is expected to double in the next 5 years<sup>1</sup>.  
32 As solar penetration continues to grow, one of the main challenges for grid integration is the  
33 variability of the solar resource as manifested in diurnal cycles and quick changes that can occur  
34 due to passing clouds. Clouds usually diminish the solar irradiance reaching the surface but clouds  
35 can also augment it, in a process known as cloud or irradiance enhancement.

36 Irradiance enhancement typically occurs during broken cloud sky conditions<sup>2</sup>, and is caused  
37 by forward scattering on thin clouds and reflection on the sides of thick clouds<sup>3,4</sup>, which not only  
38 increases the global irradiance but also modifies its spectral distribution<sup>5</sup>. While locations with  
39 high elevation near the Equator are expected to yield stronger overirradiance measurements, events  
40 have been reported all over the world. The peak measurements include 1,891 W/m<sup>2</sup> in Colorado,  
41 USA<sup>6</sup> and 1,845 W/m<sup>2</sup> in Brazil<sup>2</sup>; higher latitudes are not free of these events: 1,528 W/m<sup>2</sup> were  
42 measured in Norway<sup>7</sup>. All these values far exceed the standard testing conditions of 1000 W/m<sup>2</sup>  
43 for PV modules, and can potentially result in high output currents as well as power, both of which  
44 also depend on the operating module temperature and inverter control strategies<sup>8,9</sup>. Irradiance  
45 enhancement events last from seconds to minutes<sup>2,7,8</sup> and can cover multiple kilometers<sup>10</sup>, which  
46 can pose a problem for utility scale PV plants.

47 Inverters and the inverter strings (i.e., how many solar modules to connect in parallel) must be  
48 designed and selected such that the weather conditions at the site of interest will not exceed their  
49 rated capabilities. For this purpose, solar inverters have control strategies, and solar installations  
50 include protection fuses. Power-limiting control strategies increase the operating voltage under  
51 sustained high irradiance conditions in order to diminish the inverter input power, which as a  
52 consequence also results in a reduced operating current. This type of control could fail in specific  
53 circumstances, or have a longer time response than the fuses<sup>11</sup>. Partial shading conditions with  
54 cloud enhancement are particularly challenging and can lead to long-term inverter deterioration<sup>8</sup>.  
55 Aside from the control strategy, fuses exist in combiner boxes after the PV modules as well as on  
56 inverter DC inputs. Fuses are designed to blow when the current surpasses a given limit, reacting  
57 in the span of milliseconds. Note that fuses must sustain temperatures of up to 80°C that develop  
58 inside IP rated enclosures, which can reduce their admissible current by factors of around 0.8<sup>2</sup>.  
59 Some inverters also have software limitations which limit DC feeder current limits. In case of an

60 over-current, meaning that either the control strategy and/or the fuse failed to prevent the condition,  
61 a major inverter fault occurs. While the actual frequency of over-current faults may not be high,  
62 due to control strategies as well as heterogeneity of the PV modules and module degradation,  
63 blown fuses and inverter faults have been observed in several operational PV plants<sup>2</sup>, and are a  
64 major maintenance issue as both require manual intervention; the fuses have to be replaced, and  
65 inverters need to be reset, but there is typically no on-site staff.

66 There are some aspects in the design process that may result in having more frequent extreme  
67 conditions than anticipated. The first is related to the temporal resolution of the weather data. Ir-  
68 radiance enhancement events tend to last seconds or minutes<sup>2,12,13</sup>, while solar PV design usually  
69 considers hourly data, completely missing short-lived high currents that could lead to over-current  
70 events. A second aspect that contributes to a higher risk of damage due to overirradiance is the  
71 recent trend of increasing inverter loading ratios (ILR or DC/AC ratio) due to the declining costs  
72 of PV modules. Increasing ILR means connecting more PV modules to an inverter, which results  
73 in “clipping” or losing some power when the output of the PV modules surpasses the inverter  
74 power capacity on bright days. While these losses are thought to be compensated by a higher pro-  
75 duction during winter months and in cloudy conditions, recent measurements in Brazil suggest the  
76 opposite: undersized inverters can result in a lower annual energy generation due to overheating<sup>14</sup>.

77 The effect of time resolution has gained attention in the context of energy clipping. Kharait  
78 et al.<sup>15</sup> used 1 month of 1 minute measurements at the NIST testing site in Gaithersburg, MD, to  
79 predict energy yield and clipping losses for ILRs of 1.1, 1.3, and 1.5. Simulations in SolarFarmer  
80 showed that energy yield grows while clipping losses diminish with coarser time resolution and  
81 lower ILR, and that sensitivities are larger with higher ILR. Parikh et al.<sup>16</sup> expanded this study  
82 at the same site, for PV systems with tracking and ILR of 1.43. They used machine learning  
83 models to apply clipping loss correction factors on hourly data, reducing the PV generation bias  
84 error. Similarly, Anderson and Perry<sup>17</sup> used 29 ground stations in the US with 1 min solar data,  
85 and calculated correction factors for the clipping error of 30 min satellite data on a system with  
86 fixed tilt. This dataset was then used to train machine learning predictions in order to create a  
87 correction factor map for the continental US. This study considered a PV system with a fixed  
88 tilt of 20° and ILR of 1.4. In a study unrelated to clipping but considering non-linear effects of  
89 temporal averaging, Luoma et al.<sup>12</sup> used 1 second resolution data in San Diego, CA, to predict  
90 energy losses due to the effect of time resolution on the effective inverter efficiency, showing that  
91 10 second resolution is needed to capture the losses related to cloud enhancement events.

92 So far, these studies have not analyzed high irradiance events. The industry standard for veri-  
93 fying inverter input conditions is described by Ladd<sup>18</sup> in a SolarPro article. While the NEC 1999  
94 rule introduced a 125% multiplier, meaning that the minimum short-circuit current for selecting an  
95 inverter would be 1.25 times the short-circuit current of the PV module, the NEC 2017 rule allows  
96 simulating the local conditions on the PV modules and then using the highest 3 hour average of  
97 the modeled short-circuit current as the maximum operating condition (as long as it is higher than  
98 70% of the value obtained with the 125% multiplier). But a 3 hour average will neglect cloud  
99 enhancement events. To examine whether neglecting subhourly features is a matter of concern  
100 with respect to the existing design rules, there is a need to use high resolution data and report the  
101 strength and frequency of potentially high current events. The issue of high irradiance events is ex-  
102 pected to be of greater importance for bifacial modules. There is a brief mention of over-currents  
103 for bifacial modules in the IEA Task 13 report<sup>19</sup>, where estimates of maximum PV module current  
104 at 1 min resolution were reported to be 42% higher than the maximum 3 hour average, considering  
105 fixed tilt conditions at 3 sites in the US.

106 In this work, we compare the solar industry standard sizing calculations to subhourly solar  
107 resource simulations, and study the effect of time resolution on the simulated short-circuit and  
108 maximum power point currents, at the scale of a PV string. We consider 10 years of data with 1  
109 minute resolution at 7 SURFRAD sites in the continental US. Simulations are run in pvlib for two  
110 PV system configurations with standard and bifacial modules, considering three tilt angles as well  
111 as horizontal single axis tracking for a total of 12 scenarios. The paper is structured as follows:  
112 Section II describes the data, PV systems, and the methods. Section III shows the simulated  
113 results and their comparison to current industry standards, reporting the frequency and duration of  
114 extreme events. Section IV contains the conclusions.

## 115 **II. DATA AND METHODS**

### 116 **A. Solar and weather data**

117 We use solar and meteorological data from 7 SURFRAD stations: Bondville, IL, Boulder, CO,  
118 Desert Rock, NV, Fort Peck, MT, Goodwin Creek, MS, Penn State, PA, and Sioux Falls, SD; cor-  
119 responding to different climate conditions in the continental US. The data has 1 minute resolution,  
120 and we use historical records spanning 10 years from 2011 to 2020. The data is downsampled to

121 coarser time resolutions of 5, 15, 30, and 60 minutes.

## 122 **B. PV systems**

123 We use two reference PV systems for our simulations including monofacial and bifacial mod-  
124 ules. Since our focus is on inverter input conditions, our results will consider the expected output  
125 of a single PV string without an inverter control strategy. Typically, inverters are connected to  
126 several strings with similar setup of PV modules that are wired in parallel or in series. Tradition-  
127 ally, strings had been identical for ease of design and construction, but strings are becoming more  
128 heterogeneous as more projects are developed in complicated terrains. Each string is protected by  
129 a separate fuse. Therefore a string is the relevant unit for examining over-currents.

130 The first PV system, representing the monofacial case, is taken from Ladd<sup>18</sup>, with a total ca-  
131 pacity of 120 kW consisting of 4 inverters of 30 kW. Each inverter is fed by 5 strings of 19 Yingli  
132 YL330P-35b modules connected in series. The ILR for this system is 1.05, and the inverter has a  
133 maximum input voltage of 1,000 V and a maximum operation current of 66 A (13.2 A per string  
134 in our case). The Yingli PV module has a 15 A fuse.

135 The second PV system, representing the bifacial cases, is taken from Ayala Pelaez et al.<sup>20</sup>; it  
136 is a 200 kW DC system with 6 Chint 36 kW inverters. The bifacial modules are Silfab 285 W,  
137 and no details were reported regarding the number of modules per string nor the number of strings  
138 connected to the inverter, so we assume that each inverter is fed by 5 strings of 19 Silfab modules  
139 in series leading to 570 modules in total. Assuming a high bifacial gain (BG) of 15%, attainable  
140 in a single-axis tracking configuration for an albedo of 0.4<sup>21</sup>, the module power gives an estimated  
141 ILR of 0.84 which is low. The inverter has a maximum input voltage of 1,000 V and for 5 strings  
142 it allows a maximum input current of 14 A per string. This inverter has a 15 A fuse.

143 Each PV system is simulated for the following configurations. We consider 3 fixed-tilt angles  
144 and a case with horizontal single axis tracking (HSAT). The fixed-tilt angles are 10°, 25°, and an  
145 optimal tilt for each site. The optimal tilt corresponds to the angle that maximizes the energy yield  
146 for the monofacial module in the year 2020. The values obtained for each site are: Bondville,  
147 IL: 33°, Boulder, CO: 37°, Desert Rock, NV: 35°, Fort Peck, MT: 40°, Goodwin Creek, MS: 30°,  
148 Penn State, PA: 32°, and Sioux Falls, SD: 38°. For the bifacial modules, two albedo scenarios are  
149 considered: the annual mean of each site<sup>22</sup>, and an improved white painted concrete of 60%<sup>23</sup>, as  
150 done in the IEA Task 13 report<sup>19</sup>. This enhanced albedo may not be realistic for traditional PV

151 design, but we have included it to represent an extreme condition.

### 152 C. Simulation and current variables

153 We model the output from the PV modules using pvlib<sup>24</sup>. Measured direct and diffuse solar  
 154 irradiance is transformed to the plane of array using the Perez transposition model, and, depending  
 155 on the case, either annual mean values of albedo or an enhanced albedo of 0.6 are given for the  
 156 ground diffuse component<sup>22</sup>. Since both modules are in the CEC database, the expected module  
 157 output is obtained with the single diode CEC model, which calculates the cell temperature using  
 158 the NOCT (Nominal Operating Cell Temperature). Following Ladd<sup>18</sup>, all possible losses are set to  
 159 zero (electrical, soiling, shading, and snow), representing the worst case scenario for current output  
 160 without inverter control. For the bifacial system, the rear side irradiance is obtained with pvfactors,  
 161 a 2D method for calculating the view factors for the back side irradiance<sup>25</sup>. For bifacial irradiance,  
 162 only data for elevation angles greater than 10° was considered for the search of maximum current,  
 163 since some early times resulted in unrealistic high values. Eliminating these values is not expected  
 164 to exclude real maximum currents since the highest overirradiance events occur near noon<sup>26</sup>.

165 To compare our results with industry standards, we define the following output variables. The  
 166 125% multiplier from the NEC 2009 rule is applied to the module short-circuit current,  $I_{sc,mod}$ ,  
 167 which in these cases are 9.29 A for the Yingli and 9.49 A for the Silfab module:  $I_{125\%} = 1.25 \cdot$   
 168  $I_{sc,mod}$ , corresponding to 11.61 A and 11.86 A, respectively.

169 In practice, we would use  $I_{125\%}$  as the maximum operating condition per string to select an  
 170 inverter. To reduce inverter cost, the NEC 2017 code allows reducing the conservative 125% value  
 171 using a 3 hour average of simulated performance. We obtain the modeled (actual) short-circuit  
 172 current with the single diode CEC model from pvlib:  $I_{sc}$ . In Ladd<sup>18</sup>, the short-circuit current  
 173 was corrected using the cell temperature. Both methods yield similar results but their values are  
 174 sensitive to the module temperature coefficients  $\alpha_{sc}$  and  $\beta_{oc}$  (not shown), which can slightly differ  
 175 between the datasheet (used by Ladd) and the CEC database (used in pvlib). For consistency and  
 176 reproducibility we use the CEC database and pvlib built-in methods. We also report values of the  
 177 current at the maximum-power point,  $I_{mp}$ , which is the closest representation to typical operational  
 178 conditions. For inverters with power-limiting control strategies,  $I_{mp}$  may be lower on bright days.

179 The NEC 2017 rule suggests using the maximum 3 hour average of the modeled short-circuit  
 180 current,  $I_{sc,3h}$ . We will compare the average modeled short-circuit current and maximum-power

## Comparing solar inverter design rules to subhourly solar resource simulations

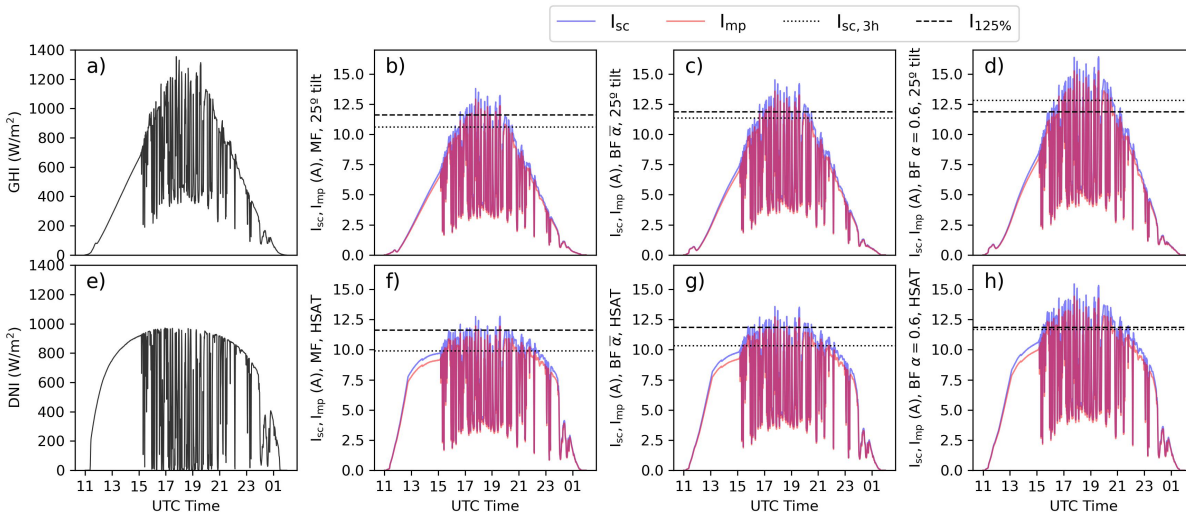


FIG. 1. Solar irradiance and modeled output currents for May 12, 2020 at Sioux Falls, showing strong variability for a large portion of the day. The first column shows the solar irradiance components: a) GHI (global horizontal irradiance) and e) DNI (direct normal irradiance). The modeled maximum-power point (red) and short-circuit (blue) currents are shown in the rest of the panels. The first row b-d) shows the values for the  $25^\circ$  tilt configuration and the second row f-h) for the HSAT configuration. The panels in the last three columns correspond to different module setups: b,f) show monofacial, c,g) bifacial with mean albedo, and d,h) bifacial with  $\alpha = 0.6$ . Horizontal lines correspond to the maximum current selected according to the 125% rule (dashed) and the maximum 3 hour average short-circuit current for the site (dotted).

181 current for different input data time resolutions as well as different averaging time windows: 5 min,  
 182 15 min, 30 min, 1 h and 3 h, for each of the sites, tilts, and module configurations.

### 183 III. RESULTS

#### 184 A. Sample results

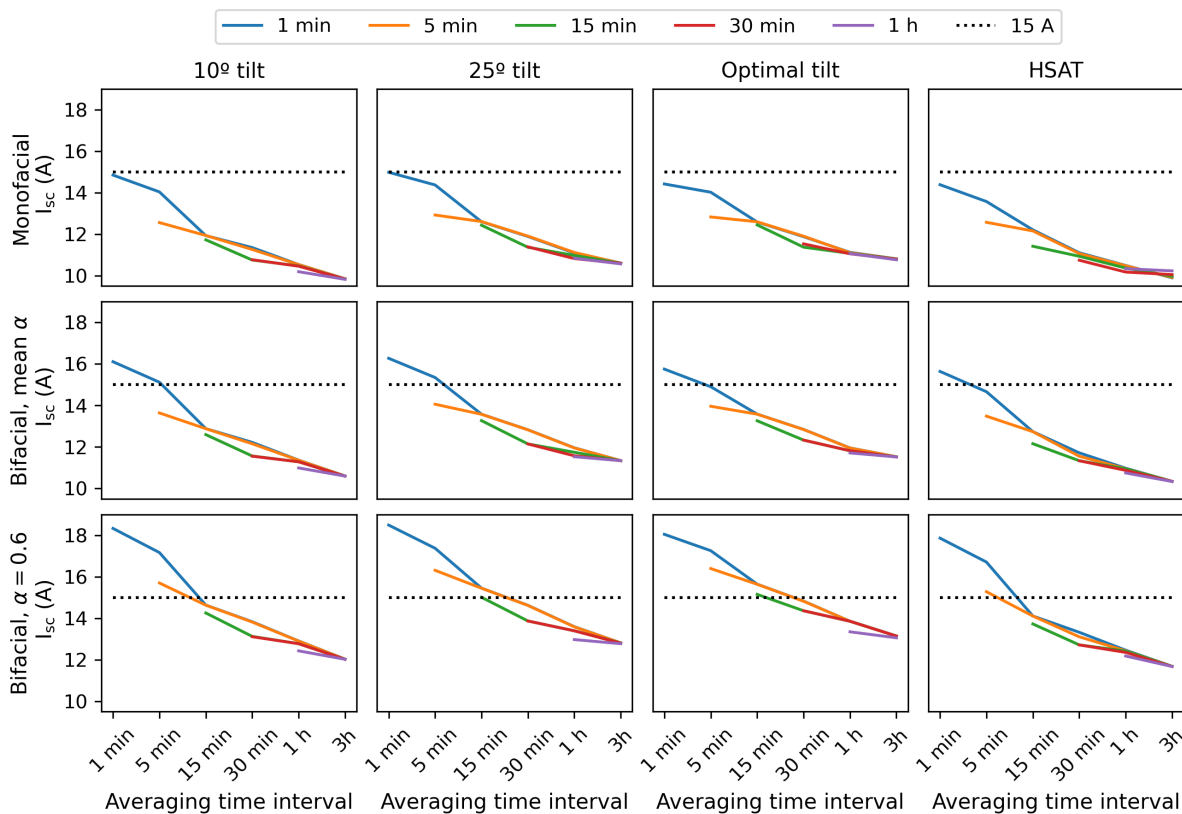
185 Fig. 1 shows the solar resource and the modeled short-circuit current ( $I_{sc}$ ) as well as the mod-  
 186 eled maximum-power point current ( $I_{mp}$ ) for May 12, 2020, at Sioux Falls, SD. This day has strong  
 187 variability, and irradiance enhancement events between 15:00-22:00 UTC.

188 The modeled  $I_{sc}$  and  $I_{mp}$  currents are shown for the  $25^\circ$  tilt configuration (Fig. 1b-d), which  
 189 closely follow the global horizontal irradiance (GHI, Fig. 1a), while the HSAT results (Fig. 1f-h)  
 190 resemble more the direct normal irradiance (DNI, Fig. 1e). The short-circuit current,  $I_{sc}$ , is by



191 definition always greater than the maximum-power point current,  $I_{mp}$ . The modeled currents are  
 192 amplified with bifacial modules, even more so when the albedo is enhanced, since the effective  
 193 irradiance reaching the modules increases. With tracking, the current peaks are lower than those  
 194 of the  $25^\circ$  fixed-tilt system throughout the day because horizontal tracking occurs at a suboptimal  
 195 tilt angle. If we had considered tilted tracking, it would have resulted in more extreme values but  
 196 two-dimensional tracking is uncommon for utility-scale plants. Lastly, the dashed and dotted lines  
 197 show the selected maximum current by using the 125% rule and the 3 hour average, respectively.  
 198 The modeled current peaks do surpass the industry standards at times, and can even be greater than  
 199 15 A, the fuse rating, for some configurations. Lastly, we note that the maximum 3 hour average  
 200 can be greater than the 125% rule for the bifacial modules with enhanced albedo.

201 **B. Maximum expected current and time resolution**



202

203 FIG. 2. Maximum short-circuit current  $I_{sc}$  for Sioux Falls, obtained from the different downsampled time-  
 204 series (1 min to 1 h), are shown as a function of the averaging time interval (1 min to 3 h).

## Comparing solar inverter design rules to subhourly solar resource simulations

205 The effect of time resolution and the averaging time interval on the maximum  $I_{sc}$  is shown  
206 in Fig. 2 for Sioux Falls. All sites show a similar behavior: the maximum currents decrease  
207 when increasing the averaging time interval, as expected. Meanwhile, for the same averaging  
208 time interval, the maximum currents found for coarser time resolution are lower or equal than  
209 the maximum found for the 1 minute averaged at that time interval. This is also expected since  
210 the downsampled timeseries may lose some extreme information while the 1 minute averaged  
211 timeseries will always contain the highest peaks, leading to the highest possible maximum.

212 In other words, coarser time resolution can underestimate the maximum values, and averaging  
213 with longer time windows certainly underestimates them. However, the difference of time reso-  
214 lution is minor when looking at 3 hour statistics, meaning that the maximum value of the 3 hour  
215 average, used for the NEC 2017 rule, is virtually identical if the original data has 1 minute or  
216 1 hour resolution. The behavior of  $I_{sc}$  and  $I_{mp}$  is similar, with the latter being always lower by  
217 around 1.5 A (see Appendix A for complementary figures).

218 Fig. 3 presents the results of the 1 minute timeseries of maximum modeled short-circuit current  
219 as a function of averaging time interval for all sites. In other words, the 12 tilt/tracking and  
220 bi/monofacial cases considered in Fig. 2 are put together in a single plot for each site. The top row  
221 in Fig. 3 shows that the modeled maximum 1 minute short-circuit current for many configurations  
222 surpasses the inverter nameplate limits (13.2 A for the monofacial, 14 A for the bifacial, and also  
223 the 15 A fuses for the monofacial module and the Chint inverter).

224 Bifacial modules reach a higher current than monofacial ones, and the enhanced albedo creates  
225 the strongest maxima for the 25° tilt. The way in which maximum currents decrease with coarser  
226 averaging time intervals is unique for each site. Some sites show a more linear behavior while  
227 others suddenly decrease at a specific averaging time interval. In the case of Sioux Falls (and  
228 also Fort Peck in Fig. 3), the sudden decrease occurs between the 5 and 15 minute intervals.  
229 This difference suggests that there is a characteristic timescale related to the duration of the strong  
230 current events for each site, which is likely to be related to the features of the clouds that lead to the  
231 strongest irradiance enhancement events at each location. Fig. 3 shows that the longest timescale  
232 is seen for Desert Rock, where the change of slope occurs at the averaging time interval of 1 h.

233 The normalized current values (second and third rows in Fig. 3) show the ratio with respect  
234 to the module's reference short-circuit current,  $I_{sc,mod}$ , and the ratio with respect to the 3 hour  
235 average maximum,  $I_{sc,3h}$  to comparing to the NEC 2009 and NEC 2017 calculations. The same  
236 plot is included for  $I_{mp}$  in Appendix A (Fig. 7).

## Comparing solar inverter design rules to subhourly solar resource simulations

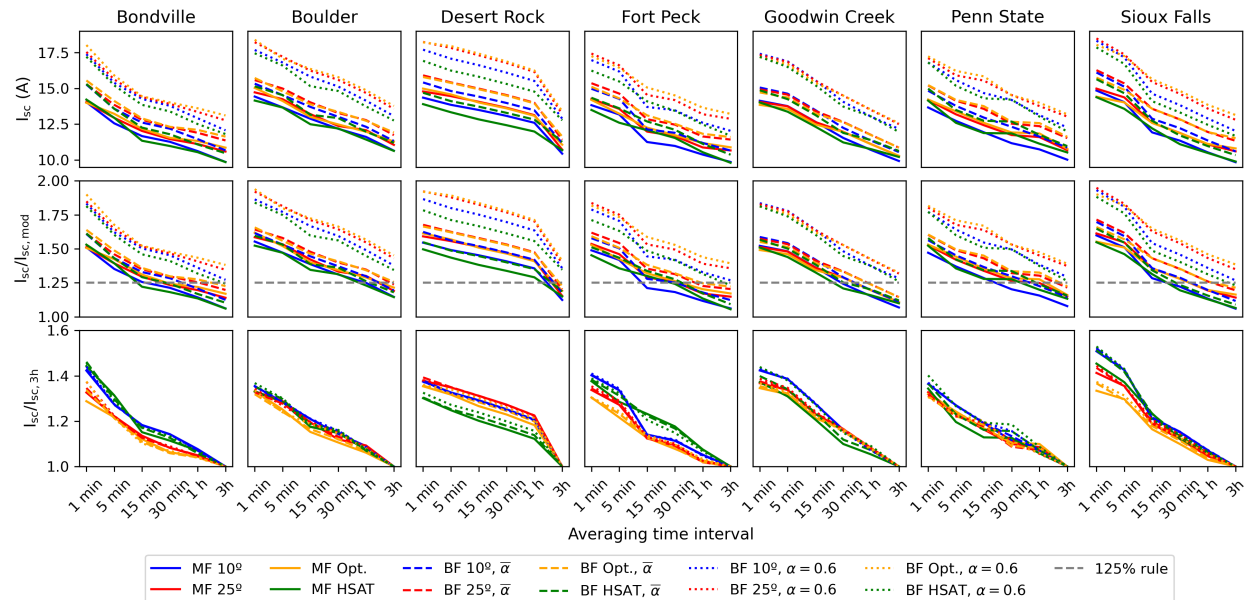


FIG. 3. Maximum modeled short-circuit current  $I_{sc}$  as a function of the averaging time interval by site, using the 1 minute resolution data. The top row shows the absolute values, the middle row shows the values normalized by the module short-circuit current  $I_{sc,mod}$  with the 125% NEC in dashed gray. The bottom row shows the values normalized by the 3 h average maximum.

237 The ratio  $I_{sc}/I_{sc,mod}$  (Fig. 3 second row) shows that for all the bifacial modules with enhanced  
 238 albedo, even the maximum 3 h average is greater than  $I_{125\%}$ , meaning that the 125% rule may  
 239 not conservative enough for those conditions, specially if the inverter has no control strategies.  
 240 Furthermore, the 125% rule is not much greater than the 3 hour averages for Boulder and Desert  
 241 Rock in the case of monofacial modules. Second, the maximum for the 1 minute data almost dou-  
 242 ble  $I_{sc,mod}$  for Sioux Falls (195%), Boulder (194%), Desert Rock (192%) and Bondville (190%)  
 243 in the bifacial cases with enhanced albedo, while for the other cases the 1 minute maximum is  
 244 at least 145% of  $I_{sc,mod}$ . For  $I_{mp}/I_{sc,mod}$  (Fig. 7 second row), the values are less extreme but still  
 245 surpass 125%: while for monofacial modules  $I_{mp}/I_{sc,mod}$  ranges from 138% at Penn State to 151%  
 246 at Boulder, the maximum values for bifacial modules reach 179% at Bondville and 178% at both  
 247 Boulder and Desert Rock.

248 The bottom row in Fig. 3 shows the ratio between the maximum averaged values and the max-  
 249 imum 3 hour average value. Here, we see that with normalization, the curves become similar and  
 250 dependent only of tilt or tracking configuration, which is expected since they determine the effec-  
 251 tive irradiance reaching the modules. The  $I_{sc}/I_{sc,3h}$  ratio is greatest for the Sioux Falls site, where

## Comparing solar inverter design rules to subhourly solar resource simulations

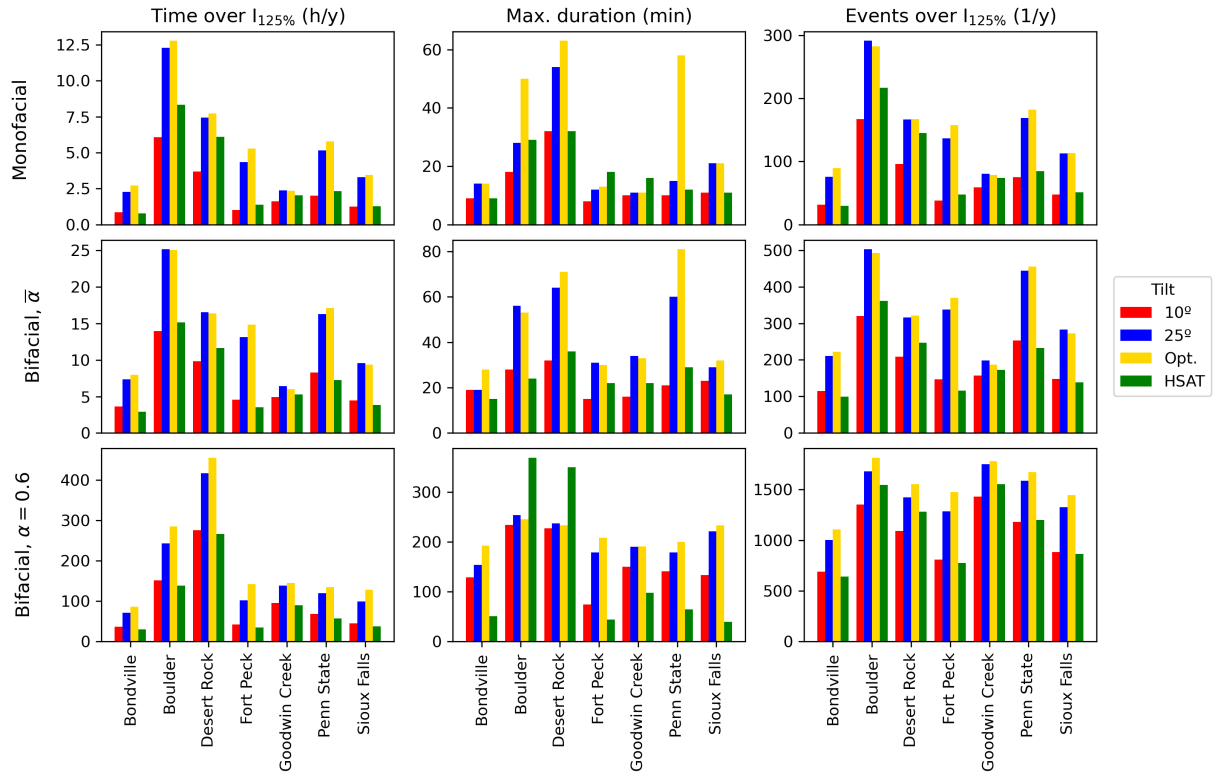


FIG. 4. Statistics of events whose short-circuit current is over the 125% rule per site and module configuration. The first column shows the aggregated time of these events per year, the second the maximum duration of the events, and the third the number of events per year. The first row corresponds to monofacial modules, the second to bifacial, and the bottom row to bifacial with enhanced albedo. The colors show the tilt or tracking configuration, with Opt. meaning optimal tilt angle.

252 the 1 minute maximum is 53% greater than the maximum 3 h average, followed by Bondville  
 253 (46%) and Goodwin Creek (44%), all of these values occurring for bifacial modules with enhanced  
 254 albedo and a HSAT configuration. Meanwhile, the minimum occurs for monofacial modules at  
 255 Bondville (29%). These values are in line with the simulated conditions and sites included in the  
 256 IEA Task 13 report<sup>19</sup>, where the same ratio reached 42% for fixed tilt conditions at 3 sites in the  
 257 US. In the case of  $I_{mp}/I_{sc,3h}$  (Fig. 7 bottom row), the maximum ratios reach 38% for Sioux Falls  
 258 while the minimum is 20% for Penn State.

## Comparing solar inverter design rules to subhourly solar resource simulations

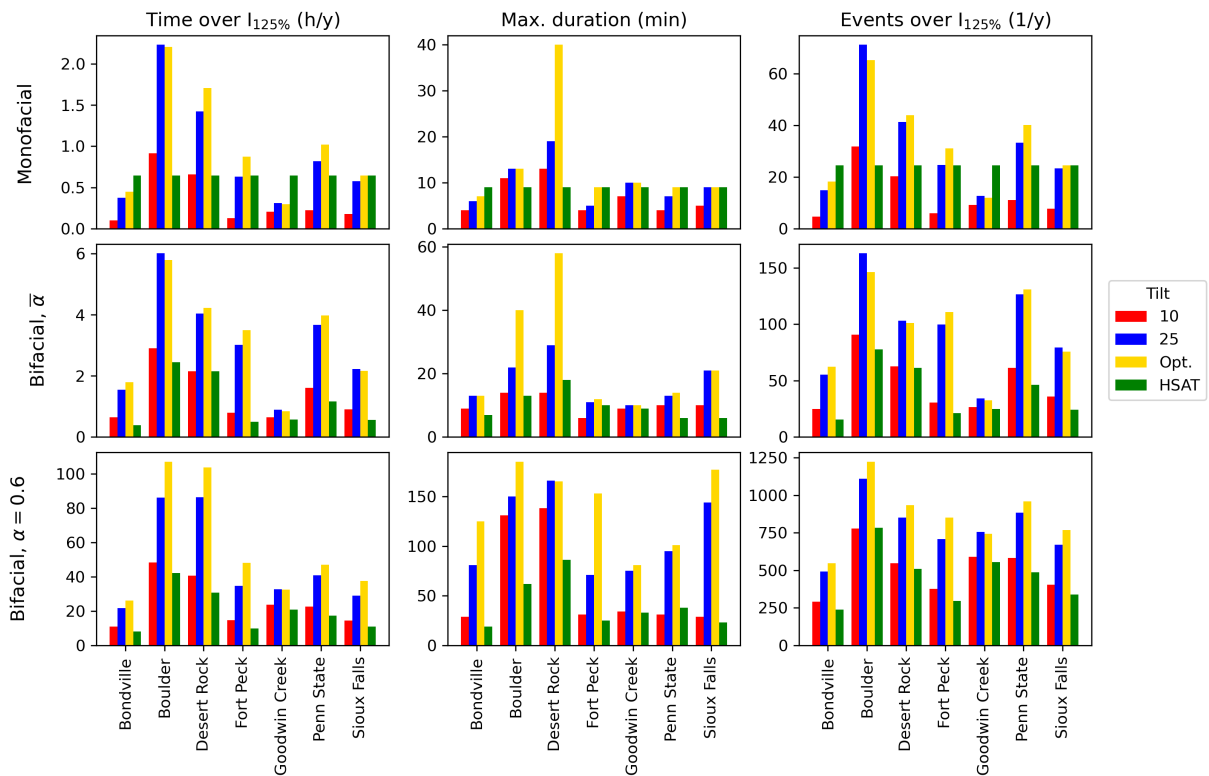


FIG. 5. Statistics of events whose maximum-power point modeled current is over the 125% rule per site and module configuration. The first column shows the aggregated time of these events per year, the second the maximum duration of single events, and the third the number of events per year. The first row corresponds to monofacial modules, the second to bifacial, and the bottom row to bifacial with enhanced albedo. The colors show the tilt or tracking configuration, with Opt. meaning optimal tilt angle.

### 259 C. Frequency and duration of high current events

260 The fact that the 125% rule is exceeded dramatically seems concerning. However, the strength  
 261 of the most extreme event in 10 years is not the only factor that affects the operation of the PV  
 262 system. Other relevant metrics are how frequent the modeled high current events over the 125%  
 263 rule are for each site, and how long they usually last. Figs. 4 and 5 show different statistics for the  
 264 events whose modeled  $I_{sc}$  and  $I_{mp}$  surpass  $I_{125\%}$ , with  $I_{mp}$  being closer to operational conditions.  
 265 The statistics in each plot include: the total time above  $I_{125\%}$  in hours per year (first column), the  
 266 maximum duration of these events in minutes (mid column), and the number of events per year  
 267 (third column).

268 As expected, the high current events may occur more frequently for higher tilt angles (blue and

269 yellow bars), and for the locations with a more abundant solar resource: Boulder and Desert Rock.  
270 While the modeled  $I_{sc}$  in a PV plant with monofacial modules at Goodwin Creek might surpass  
271 the 125% rule for around 2 hours per year, another at Boulder could reach 12 hours per year. As  
272 we change to bifacial modules with enhanced albedo, the frequency increases, reaching up to 456  
273 hours per year at Desert Rock (equivalent to full 38 solar days).  $I_{mp}$  in Fig. 5 gives an idea of  
274 possible operational failures. The numbers are about a third of the statistics based on the modeled  
275  $I_{sc}$ . The worst case in monofacial modules is Boulder with only 2.2 hours per year and bifacial  
276 with enhanced albedo at 134 hours (equivalent to 5.6 days).

277 In terms of duration, the longest events where the modeled  $I_{sc} > I_{125\%}$  for the monofacial cases  
278 last between 8 and 63 minutes at Fort Peck and Desert Rock, respectively. For the bifacial modules  
279 with average site albedos, the range is between 15 minutes at both Bondville and Fort Peck, and  
280 81 minutes at Penn State. Lastly, the bifacial modules with enhanced albedo result in the longest  
281 events between 39 minutes for Sioux Falls and 369 (over 6 h) at Boulder, which are probably  
282 not related to irradiance enhancement but extended favorable conditions. In fact, note that the  
283 longest events for enhanced albedo occur at Boulder and Desert Rock for the HSAT configurations,  
284 meaning that tracking is playing an important role in augmenting the incident irradiance over the  
285 modules throughout the day, not just for irradiance enhancement events but mean irradiance as  
286 well. The extreme events based on modeled  $I_{mp} > I_{125\%}$  show a similar behavior, but note that in  
287 these cases the longest events are not for the HSAT configuration. Here, the longest events last 40  
288 min for the monofacial modules at Desert Rock, 58 min for the bifacial modules with site mean  
289 albedo at Desert Rock, and 185 min for the bifacial modules with enhanced albedo at Boulder.  
290 The maximum duration based on  $I_{mp}$  is around half that based on  $I_{sc}$ . As we previously saw in Fig.  
291 3, the 125% rule determines a low requirement when comparing to the 3 h maximum average for  
292 bifacial modules with enhanced albedo, so the long duration of the events is also related to having  
293 too low of a threshold, in proportional terms.

294 Lastly, the number of events per year gives an idea of the possible maintenance frequency such  
295 as replacing fuses for inverters without control strategies. For both modeled  $I_{sc}$  and  $I_{mp}$ , Boulder  
296 leads for mono and bifacial modules, at either 25° or its optimal tilt setup. The maximum number  
297 of events for  $I_{sc} > I_{125\%}$  are 291 for monofacial modules, 503 for bifacial with mean site albedo,  
298 and 1,816 for bifacial with enhanced albedo. Meanwhile, the maximum number of events for  
299 modeled  $I_{mp} > I_{125\%}$  are 71 for monofacial modules, 163 for bifacial with mean site albedo, and  
300 1,224 for bifacial with enhanced albedo. The number of extreme events based on modeled  $I_{mp}$

301 range between 24-67% of those based on  $I_{sc}$ .

302 Both the mean time over the 125% rule, the maximum duration of the extreme events, and  
303 the mean number of events per year help us to quantify the possible impact of the times where a  
304 PV string may deliver a strong current, complementing the previously provided maximum short-  
305 circuit current and maximum power-point current. This is especially important for some sites.  
306 While Sioux Falls presented the strongest 1 min maximum values, now we see that those events  
307 are not as frequent as in other locations like Boulder. Additional parameters related to frequency  
308 could also be helpful for inverter selection if the goal was to minimize the total time of failure  
309 instead of no failure at all in cases without power-limiting control strategies, or for choosing a tilt  
310 angle instead of a tracking system when working with bifacial modules.

#### 311 IV. CONCLUSIONS

312 We have analyzed the possible impacts of overirradiance events in solar plants by reporting  
313 the frequency and duration of simulated high current outputs of a PV string and comparing them  
314 with inverter selection standards, considering several configurations and sites in the US. The study  
315 also covered the effect of time resolution and averaging on the modeled results. We used 10 years  
316 of 1 minute solar data for 7 sites in the SURFRAD network, and simulated the short-circuit and  
317 maximum-power point currents using pvlib. Modeled currents were compared with the industry  
318 standards NEC 2009 and NEC 2017, corresponding to the 125% rule and the 3 hour average  
319 maximum, respectively.

320 The maximum modeled short-circuit current decreases with time resolution and averaging and  
321 the shape of the decay varies by site. The 3 hour average maximum short-circuit current is insen-  
322 sitive to the original data time resolution. The 1 minute maximum short-circuit current was the  
323 strongest at Sioux Falls for the 25° tilt and bifacial module with enhanced albedo, and it greatly  
324 surpassed the 125% rule for all cases. In some cases, the 1 minute maximum even surpassed the  
325 inverter nameplate maximum and string fuses. For the bifacial modules with enhanced albedo, the  
326 3 hour maximum was already greater than the 125% rule. This suggests that – even for coarse res-  
327 olutions – 125% may not be a suitable rule for selecting an inverter without power-limiting control  
328 for bifacial modules. The frequency of the events over the 125% rule was largest at the sites with  
329 more solar resource: Boulder and Desert Rock. The longest extreme events were over 6 hour long  
330 for bifacial modules with enhanced albedo and tracking.

331 The current industry standards for selecting inverters based on the 125% rule or 3 hour averages  
332 were found to be lower than the maximum modeled currents caused by short and strong events of  
333 overirradiance. While for monofacial modules the 3 hour average maximum is less strict than the  
334 125% rule, this was not true for bifacial modules. If the goal was to create a rule that could avoid  
335 any possible strong 1 minute event, either a 200% rule based on the module's short-circuit current  
336 or 1.5 times the 3 hour maximum average, which could be derived from hourly data, would avoid  
337 any large current event. Still, if 1 min resolution data is available, either from measurements or  
338 more recent satellite-derived commercial products, it will still be beneficial to do a high resolution  
339 simulation for a more informed design.

340 We would like to note that the analysis performed used data that represents the behavior of a  
341 single point in space. While a large solar plant is known to smooth the incoming strong irradiance  
342 by geographic diversity effect related to covering a large area, a single string might not represent  
343 significant geographic diversity to smooth the timeseries, and follow the results presented herein.

344 Lastly, inverter power-limiting control deviates from the maximum-power point to higher volt-  
345 age operating points<sup>8,10</sup>, which usually leads to a lower operating current. Still, this type of control  
346 strategies may fail under partial cloudy skies, and existing PV plants with maximum-power track-  
347 ing algorithms are likely to continue failing. Future work could add realism to these type of  
348 diagnostics by estimating the derating of fuses due to high temperatures, or to include an inverter  
349 model in order to simulate the actual inverter input current.

## 350 ACKNOWLEDGMENTS

351 MZZ thanks the Faculty of Physical and Mathematical Sciences at Universidad de Chile for a  
352 faculty incorporation grant.

## 353 DATA AVAILABILITY STATEMENT

354 Solar data are available at the SURFRAD website: [https://gml.noaa.gov/aftp/data/  
355 radiation/surfrad/](https://gml.noaa.gov/aftp/data/radiation/surfrad/). The code used in this study is available at [https://github.com/  
356 mzamora/InverterEnhancement](https://github.com/mzamora/InverterEnhancement).



357 **REFERENCES**

358 <sup>1</sup>International Energy Agency, “Renewables 2021,” Tech. Rep. (2021).

359 <sup>2</sup>L. R. do Nascimento, T. de Souza Viana, R. A. Campos, and R. Rütger, “Extreme solar overir-  
360 radiance events: Occurrence and impacts on utility-scale photovoltaic power plants in Brazil,”  
361 *Solar Energy* **186**, 370–381 (2019).

362 <sup>3</sup>Z. K. Pecenek, F. A. Mejia, B. Kurtz, A. Evan, and J. Kleissl, “Simulating irradiance enhance-  
363 ment dependence on cloud optical depth and solar zenith angle,” *Solar Energy* **136**, 675–681  
364 (2016).

365 <sup>4</sup>G. H. Yordanov, “A study of extreme overirradiance events for solar energy applications using  
366 NASA’s I3RC Monte Carlo radiative transfer model,” *Solar Energy* **122**, 954–965 (2015).

367 <sup>5</sup>M. A. Zamalloa-Jara, M. Sevillano-Bendezú, C. Ulbrich, G. Nofuentes, R. Grieseler, and J. A.  
368 Töfflinger, “Overirradiance conditions and their impact on the spectral distribution at low- and  
369 mid-latitude sites,” *Solar Energy* **259**, 99–106 (2023).

370 <sup>6</sup>C. A. Gueymard, “Cloud and albedo enhancement impacts on solar irradiance using high-  
371 frequency measurements from thermopile and photodiode radiometers. Part 1: Impacts on global  
372 horizontal irradiance,” *Solar Energy* **153**, 755–765 (2017).

373 <sup>7</sup>G. H. Yordanov, O.-M. Midtgård, T. O. Saetre, H. K. Nielsen, and L. E. Norum, “Overirradi-  
374 ance (cloud enhancement) events at high latitudes,” in *2012 IEEE 38th Photovoltaic Specialists  
375 Conference (PVSC) Part 2* (2012) pp. 1–7.

376 <sup>8</sup>M. Järvelä and S. Valkealahti, “Operation of a PV power plant during overpower events caused  
377 by the cloud enhancement phenomenon,” *Energies* **13** (2020), 10.3390/en13092185.

378 <sup>9</sup>K. Lappalainen and S. Valkealahti, “Experimental observations about the cloud enhancement  
379 phenomenon on PV strings,” in *8th World Conference on Photovoltaic Energy Conversion*  
380 (2022) pp. 1354 – 1358.

381 <sup>10</sup>K. Lappalainen and J. Kleissl, “Analysis of the cloud enhancement phenomenon and its effects  
382 on photovoltaic generators based on cloud speed sensor measurements,” *Journal of Renewable  
383 and Sustainable Energy* **12**, 043502 (2020).

384 <sup>11</sup>“New study claims PV industry is neglecting overirradiance issues,” (2023).

385 <sup>12</sup>J. Luoma, J. Kleissl, and K. Murray, “Optimal inverter sizing considering cloud enhancement,”  
386 *Solar energy* **86**, 421–429 (2012).

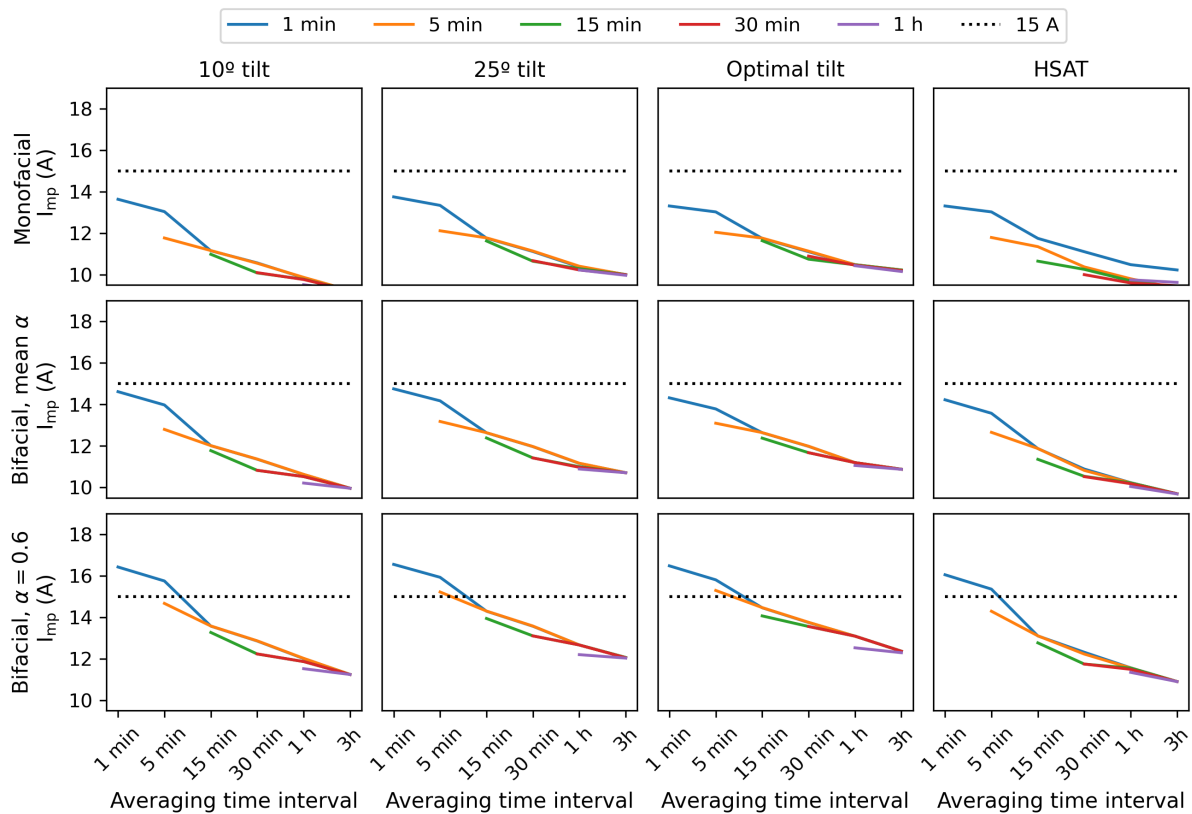
- 387 <sup>13</sup>M. Zamora Zapata, E. Wu, and J. Kleissl, “Irradiance enhancement events in the coastal strato-  
388 cumulus dissipation process,” in *Solar World Congress, Santiago, Chile, International Solar*  
389 *Energy Society* (2019).
- 390 <sup>14</sup>L. Toreti Scarabelot, G. Arns Rampinelli, and C. R. Rambo, “Overirradiance effect on the  
391 electrical performance of photovoltaic systems of different inverter sizing factors,” *Solar Energy*  
392 **225**, 561–568 (2021).
- 393 <sup>15</sup>R. Kharait, S. Raju, A. Parikh, M. A. Mikofski, and J. Newmiller, “Energy yield and clipping  
394 loss corrections for hourly inputs in climates with solar variability,” in *2020 47th IEEE Photo-*  
395 *voltaic Specialists Conference (PVSC)* (2020) pp. 1330–1334.
- 396 <sup>16</sup>A. Parikh, K. Perry, K. Anderson, W. B. Hobbs, R. Kharait, and M. A. Mikofski, “Valida-  
397 tion of subhourly clipping loss error corrections,” in *2021 IEEE 48th Photovoltaic Specialists*  
398 *Conference (PVSC)* (2021) pp. 1670–1675.
- 399 <sup>17</sup>K. Anderson and K. Perry, “Estimating subhourly inverter clipping loss from satellite-derived  
400 irradiance data,” in *2020 47th IEEE Photovoltaic Specialists Conference (PVSC)* (2020) pp.  
401 1433–1438.
- 402 <sup>18</sup>C. Ladd, “Simulating NEC voltage and current values,” *Solar professional magazine*, 12–18  
403 (2008).
- 404 <sup>19</sup>J. Stein, C. Reise, J. B. Castro, G. Friesen, G. Maugeri, E. Urrejola, and S. Ranta, “Bifacial  
405 photovoltaic modules and systems: Experience and results from international research and pilot  
406 applications,” Tech. Rep. (IEA, 2021).
- 407 <sup>20</sup>S. Ayala Pelaez, C. Deline, P. Greenberg, J. S. Stein, and R. K. Kostuk, “Model and validation  
408 of single-axis tracking with bifacial PV,” *IEEE Journal of Photovoltaics* **9**, 715–721 (2019).
- 409 <sup>21</sup>LG, “Bifacial design guide,” Tech. Rep. (2017).
- 410 <sup>22</sup>B. Marion, “Albedo data sets for bifacial PV systems,” in *2020 47th IEEE Photovoltaic Special-*  
411 *ists Conference (PVSC)* (2020) pp. 0485–0489.
- 412 <sup>23</sup>Solar World, “Calculating the additional energy yield of bifacial solar modules,” (2016).
- 413 <sup>24</sup>W. F. Holmgren, C. W. Hansen, and M. A. Mikofski, “pvlib python: a python package for  
414 modeling solar energy systems,” *Journal of Open Source Software* **3**, 884 (2018).
- 415 <sup>25</sup>M. A. Anoma, D. Jacob, B. C. Bourne, J. A. Scholl, D. M. Riley, and C. W. Hansen, “View  
416 factor model and validation for bifacial PV and diffuse shade on single-axis trackers,” in *2017*  
417 *IEEE 44th Photovoltaic Specialist Conference (PVSC)* (2017) pp. 1549–1554.

418 <sup>26</sup>A. Castillejo-Cuberos and R. Escobar, “Understanding solar resource variability: An in-depth  
 419 analysis, using Chile as a case of study,” *Renewable and Sustainable Energy Reviews* **120**,  
 420 109664 (2020).

421 <sup>27</sup>I. Santiago, J. L. Esquivel-Martin, D. Trillo-Montero, R. J. Real-Calvo, and V. Pallarés-López,  
 422 “Classification of Daily Irradiance Profiles and the Behaviour of Photovoltaic Plant Elements:  
 423 The Effects of Cloud Enhancement,” *Applied Sciences* **11**, 5230 (2021).

424 **Appendix A: Complementary statistics for  $I_{mp}$**

425 The following Figs. 6 and 7 represent the same behavior shown for  $I_{sc}$  in Figs. 2 and 3 but for  
 426 the modeled maximum-power point current  $I_{mp}$ .



427

428 FIG. 6. Maximum current at the maximum-power point  $I_{mp}$  for Sioux Falls, obtained from the different  
 429 downsampled timeseries (1 min to 1 h), are shown as a function of the averaging time window (1 min to 3  
 430 h).  
 431

432

## Comparing solar inverter design rules to subhourly solar resource simulations

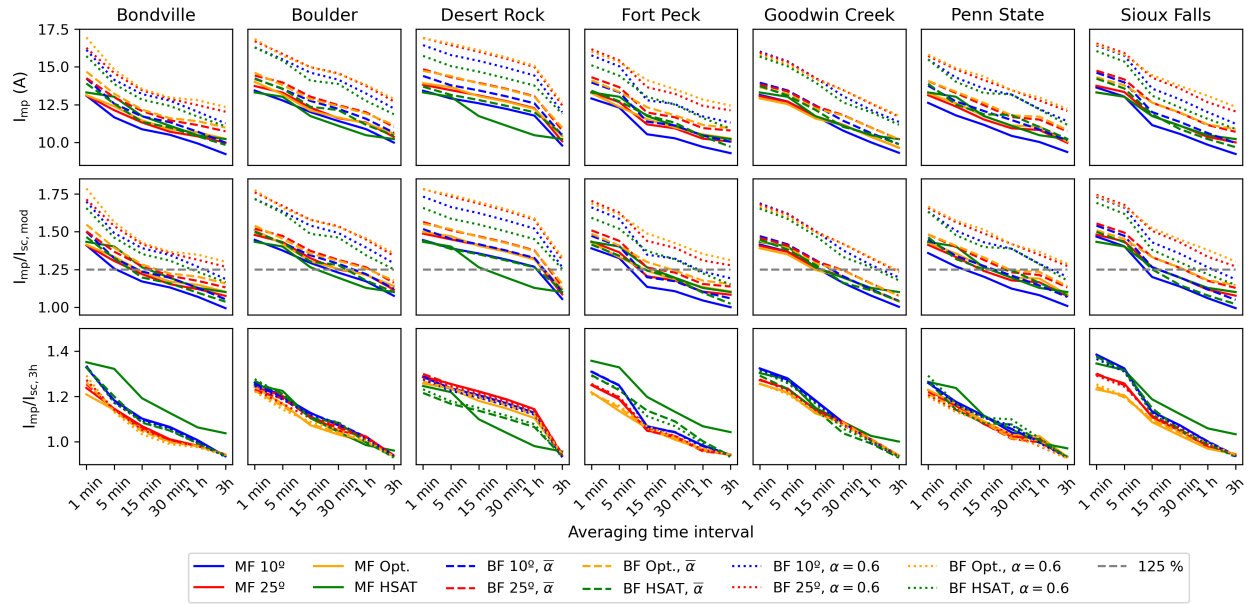


FIG. 7. Maximum current at the maximum-power point  $I_{mp}$  as a function of the averaging time window per site, using the 1 minute resolution data. The top row shows the absolute values highlighting the 15 A in dashed gray, the middle row shows the values normalized by the module short-circuit current  $I_{sc,mod}$ , and the bottom row shows the values normalized by  $I_{sc,3h}$ .